Numerical Methods in Civil Engineering, 6-4 (2022) 67-77

Numerical Methods in Civil Engineering

Journal Homepage: https://nmce.kntu.ac.ir/

Investigation of the performance of self-centering steel plate shear walls under fire loading

Nader Fanaie* **and Mahtabsadat Razavi****

ARTICLE INFO

RESEARCH PAPER

Article history:
Received:
January 2022.
Revised:
January 2022.
Accepted:
February 2022.

Keywords:
Self-centering connections, self-centering steel plate shear wall, finite element, post-fire earthquake, energy dissipation

Abstract:

A potential multi-hazard scenario for buildings is the sequential occurrence of fire and earthquake. This scenario is possible if an initial seismic event triggers fire and a subsequent aftershock occurs. To study the post-fire seismic performance, a numerical study is presented on a two-story self-centering steel plate shear wall. This system consists of post-tensioned elements such as strands and bars to reduce the residual drift in the structure and energy dissipator devices to dissipate the seismic input energy. This paper assesses the seismic behavior of self-centering steel plate shear walls after fire loading and proposes modifications to their structural details so that fire robustness can be achieved in addition to seismic resilience. This system is simulated using the finite element method (FEM) and is verified based on available experimental results. Then, fire loading is applied, and results are compared for protected and unprotected models. Results showed that protecting steel members with fire-resistant coating can significantly improve the post-fire seismic performance of the system. The protected models reveal higher lateral strength relative to unprotected models with an increase in temperature. The maximum lateral strength of the self-centering steel plate shear wall model with shielded steel web panels, the model with shielded strands, and the model with both shielded strands and steel web panels are respectively 56%, 21%, and 61% greater than the model without fire-resistant coating at 700 °C.

1. Introduction

The moment frames with welded connections, which were used in the regions as earthquake-resistant structures, experienced brittle fractures in beam-to-column connections during the earthquakes of Northridge 1994 and Kobe 1995 [1]. Inspired by this event, researchers carried out investigations in conjunction with improving the seismic performance of the connections. Among these, the beam-column connection using reduced flange, commonly known as reduced beam section (RBS) moment connections, the reinforced connection with cover and side plates, and connections with self-centering capabilities could be pointed out [2]. To prevent the yielding and local buckling of the main members that lead to permanent deformation in the primary structural members, buildings should be designed so that damage is limited to members that could be simply repaired or replaced. The structural systems that provide this possibility are referred to as self-centering systems.

Self-centering connections in steel moment frames and shear walls are designed to omit inelastic deformations and residual drift in structural members caused by earthquakes. This ductile behavior is generated due to the creation of a gap at the post-tensioned (PT) connection. The ductility demand of this system against lateral forces is very high. Unlike steel frames, which are established based upon the ductility and strength of the materials of structural members, the behavior of self-centering structures is not controlled by the ductility demand of the materials. Energy

* *Corresponding Author: Associate Professor, Faculty of Civil Engineering, K. N. Toosi University of Technology, Tehran, Iran. E-mail: fanaie@kntu.ac.ir*
** *Graduate Student, Faculty of Civil Engineering, K. N. Toosi University of Technology, Tehran, Iran. E-mail: mahtabrazavi@email.kntu.ac.ir*

[DOR: 20.1001.1.23454296.2022.6.4.8.5]
[DOI: 10.52547/nmce.6.4.67]

dissipation in self-centering structures under seismic loading does not occur by failure in the primary structural members but occurs via elements deployed as energy dissipators that could be substituted in case of failure.

The self-centering steel plate shear wall (SC-SPSW) is a new seismic load-resisting system that combines the strength and stiffness properties of the SPSW with the re-centering capabilities of post-tensioned (PT) beam-to-column connections.

Through the combination with self-centering (SC) capacity that is based on post-tension steel strands to restore the structure to its original state after an earthquake, the characteristics of the SPSW system could be enhanced. Figure 1 illustrates an SPSW system with self-centering capability composed of web plates, post-tensioned (PT) connections, horizontal boundary elements (HBE), and vertical boundary elements (VBE) [3]. The models offered for SC-SPSWs are different in terms of energy dissipator elements and elements providing self-centering capability.

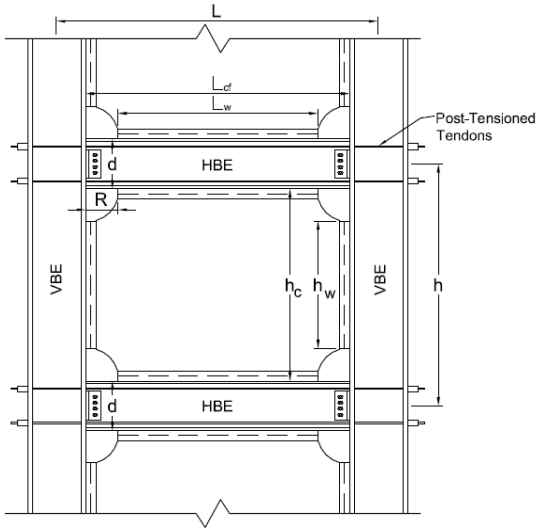

Fig. 1: Self-centering steel plate shear wall setup

From 2000 until now, numerous researchers have performed experimental and analytical investigations on the utilization of self-centering mechanisms in members of precast reinforced concrete structures. Some examples of these can be noted as follows: In 2000, a hybrid system of steel beams and reinforced concrete shear walls, where the self-centering property was also taken into account, was analytically studied. Regardless of considering the continuation of the steel beams inside the wall, their connection was established via post-tensioned strands and top-and-seat-angle wide flange (WF) beam-to-column connections as energy dissipators, and an analytical model was suggested for predicting the behavior of the system mentioned above and its design [4]. In 2001, a novel style of structural systems to reduce the damages caused by earthquakes was proposed. This system embraced a reinforced precast concrete shear wall (PCSW) structure and post-tensioned elements, which led to substantial compressive strains in the wall toes under the influence of lateral force following the formation of a seam at the point of connection of the wall to the foundation. The survey results indicated that the relative permanent displacement of the system in strong earthquakes is insignificant [5].'

In 2007, a precast reinforced concrete wall with the rocking motion capability around the connection point to the foundation was experimentally explored. The self-centering feature was supplied by the gravitational forces and the elastic force caused by the post-tensioned strands as a result of applying lateral force and opening at the foundation. The conventional steel reinforcing bars that were deployed at the connection point of the foundation were employed for providing energy dissipation in the system so that the rebars were yielded due to the wall opening, and energy was favorably dissipated [6].

Furthermore, a system was introduced in 2010 following the listed studies, incorporating hollow precast wall panels and post-tension strands to provide the self-centering capability. The bars, which were post-tensioned at the rate of 50%, were applied for energy dissipation. Until reaching the relative displacement of 4%, the tested walls remained elastic, and inelastic deformations only occurred in the energy-dissipating elements [7].

Clayton et al. in 2012 presented the seismic design and performance of SC-SPSWs using time-history analysis [8]. In this system, web plates are taken into account as energy-dissipating elements and enter the plastic range while the beams and columns remain elastic.

Nobahar et al., in 2019, carried out investigations on a promising post-tensioned self-centering yielding braced system (PT-SCYBS), comprising two main types of components: post-tensioned wires, exhibiting desirable self-centering properties, and steel bars, providing energy dissipation capacity. In this survey, the residual drift of the PT-SCYBS was compared with those of moment-resisting frame (MRF) systems. Comparing the results of the PT-SCYBSs and MRFs, it can be concluded that the residual drift decreased by 96% and 77% for the 3- and 9-story buildings, respectively [9].

Liu et al., in 2020, conducted an experimental study on component performance in steel plate shear walls with self-centering energy dissipation braces (SPSW-SCEDB) [10]. A one-story shear wall having an opening was designed and tested in this research. The results revealed that this system has a relatively high initial stiffness and exhibits a flag-shaped hysteretic response. In addition, concentric braces reduce stiffness drop in the system and enhance strength against lateral loads.

[DOR: 20.1001.1.23454296.2022.6.4.8.5]
[DOI: 10.52547/nmce.6.4.67]

[DOR: 20.1001.1.23454296.2022.6.4.8.5]

[DOI: 10.52547/nmce.6.4.67]

Hitaka and Matsui, in 2003, conducted a study to reflect the ductility of a self-centering modular panel with slit steel shear walls (SCMP-SW) [11]. The system is a new seismic load-resisting structural component that combines re-centering capabilities and energy dissipation ability while applying lateral load. The self-centering modular panel is designed as a post-tensioned steel moment-resisting frame and generates re-centering capabilities in the system. Alongside these panels, the slit walls are intended to serve as replaceable fuse elements for energy dissipation purposes [12]. Based on Hitaka and Matsui's experiments, the moment connection between the slits causes a desirable ductility in the shear wall. When applying lateral loads, the slit steel shear walls experience inelastic deformations. Elastic deformations result in generating a relative residual displacement (residual drift) in the structure. Therefore, creating a self-centering property in these systems is very critical.

Per the studies carried out by Wang et al. in 2018, the SCMP-SW system has a flag-shaped hysteresis response, which is very close to its ideal response. The behavior of post-tensioned strands is identical to that of pre-tensioned strands in the SCMP-SW system. Hence, the initial force in post-tensioned strands is equal to the post-tensioning force, and this force enhances by opening the gap in the connection. Using the flexural strength of moment connections, the slit walls are resistant to lateral loads and perform the energy dissipation through inelastic deformation at the top and bottom of the moment connections between the slits.

Several studies have been conducted on the influence of fire on the lateral strength of buildings. Al Kajbaf and Fanaie [13], in 2018, did a numerical analysis of self-centering steel moment connections to investigate the effect of fire loading on the lateral strength of the connection. They used finite element modeling to compare the moment capacity of the connection with protected strands to that of the model without protection. They conducted a static push-over analysis at an elevated temperature, and the results revealed that the maximum moment capacity of the connection with protected strands is 88% higher than that of the model with unprotected strands at 700 *°C*.

Ni and Birely [14], in 2018, conducted a numerical study to investigate the impact of fire damage on the lateral load resistance of flexure-controlled RC structural walls. Results indicate that fire damage decreases the load-bearing capacity and the stiffness of RC walls under reversed-cyclic loads.

Mazza [15], in 2017, carried out investigations on the post-fire seismic performance of reinforced concrete framed structures with fire-induced damage during seismic aftershocks. A numerical study was presented on six-story reinforced concrete framed structures composed of a basement with elastomeric bearings and five stories above the ground. Three fire scenarios were compared, selecting the base-isolated level, first, and fifth levels of the superstructure as fire compartments, and the transient response of the elastomeric bearings was compared with the steady response.

Jin et al. [16], in 2021, performed a study on the post-fire seismic behavior of RC short columns. A 3-D meso-scale model of reinforced concrete short columns under cyclic loading was established, and results indicate that the degradation of energy dissipation capacity of columns after fire exposure is different from that at room temperature.

2. Ideal Response of a Self-Centering System

The ideal hysteresis response for all SC-SPSW systems is flag-shaped. This ideal curve can be observed in Fig. 2 (a).

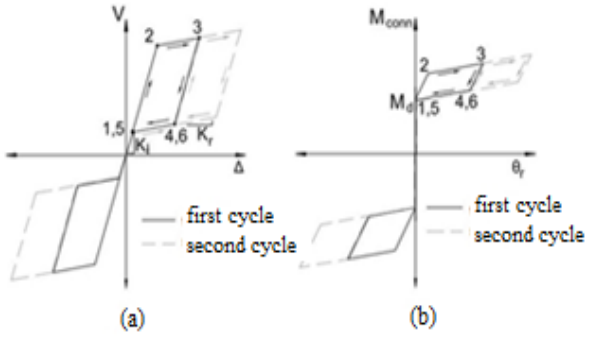

Fig. 2: Idealized cyclic behavior of (a) SC-SPSW, (b) PT connection

As previously pointed out, the primary strength of the system and energy dissipation is supplied by the steel plate shear wall, and post-tensioned (PT) connections provide the self-centering capability for the system. The SC-SPSW system has an initial stiffness, K_i, while the lateral load is applied. This stiffness is equal to the initial stiffness of the conventional shear wall system. After the connection enters the decompression limit state (limit state 1 in Fig. 2 (a), the steel plate shear wall (SPSW) resists the lateral load by generating a tensile field so that the plate is ultimately yielded (limit state 2 in Fig. 2 (a). As can be observed, the structure's lateral stiffness considerably declines after this limit state. The elastic stiffness of the plate is restored during the unloading cycle (limit state 3 in Fig. 2 (a). After full unloading (limit state 4 in Fig. 2 (a), the post-tensioned (PT) connections are compressed again and result in the creation of a re-centering stiffness, K_r, and reduce the displacement in the structure to zero (limit state 5 in Fig. 2 (a) [8].

Regardless of the compressive strength of the SPSW during unloading, the re-centering stiffness, K_r, is achieved from Eq. (1) [8].

$$K_r = \frac{\sum k_d^\theta}{H^2} \quad (1)$$

In which H is the total height of the structure, and $\sum k_d^\theta$ is the sum of the post-tensioned (PT) connection's rotational stiffness, calculated from Eq. (2) [8].

$$k_d^\theta = \frac{d^2}{2}\left(\frac{k_{PT}k_{HBE}}{k_{PT}+k_{HBE}}\right) \quad (2)$$

Where d is the depth of the HBE at the connection and k_{PT} and k_{HBE} are the axial stiffness of all the PT strands and the HBE at a particular level, respectively. In the case that only the tensile behavior of the SPSW is taken into account, and it is supposed that the stress distribution in the web plate is uniform, the steel plate shear wall should reach maximum equivalent plastic strain following several loading cycles after the decompression limit state (limit state 6 in Fig. 2 (a) [8].

The curves presented in Fig. 2 are formed based on the elastic-perfectly plastic (EPP) behavior without considering the compressive strength of the steel plate shear wall. For simplification, these assumptions have been generated. However, if the simplification assumptions are not carried out, Fig. 2 becomes complex [8].

3. Finite Element Modeling

The self-centering steel plate shear wall (SC-SPSW) system, which was experimentally evaluated by Clayton et al. [17], was chosen in this study, and its 3D finite element model was developed using the Abaqus software. The experimental configuration of the model is displayed in Fig. 3.

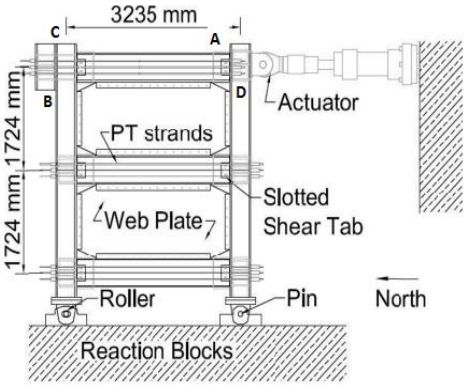

Fig. 3: Schematic of experiment setup

The two-story shear wall model embraces three horizontal boundary elements (HBE) with a cross-section of 14 × 90 W, two vertical boundary elements (VBE) with a cross-section of 14 × 132 W, post-tensioned (PT) strands, and web plates. At the level of each story, eight post-tensioned (PT) strands are utilized. The center to center spacing of the columns and beams are 3235 and 1724 mm, respectively. As stated before, the beams and columns remain in an elastic state in this system, and no plastic hinges are shaped in them; thus, the wire element is employed for their modeling.

The stress contour of the finite element model is shown in Fig. 4.

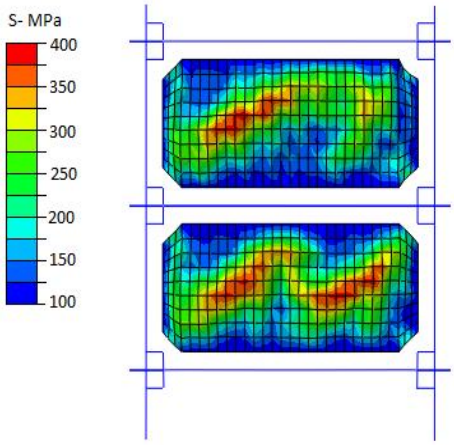

Fig. 4: Stress contour in the finite element model

According to the yield stress of frame members, which is 345 MPa, there are no regions of high stresses that lead to the plastic hinges in beams and columns.

Because there are rocking connections and they are not fixed connections, the depth of the beam and column should be introduced to the software. The rigid offset element was exploited to model the beam and column depth. The post-tensioned (PT) strands are braced to the outer edge of the column so that conditions for rocking connection are provided. As steel panels are intended to serve energy dissipation of the system, the shell element was applied for their modeling. The steel panels are placed exactly below the beam flanges, and their dimensions in each story are 2117 × 1367, with a thickness of 1.5 mm.

A small out-of-plane deformation is applied using buckling analysis to generate the initial defect in the steel panels, and the outcomes are put on in the model analysis.

3.1. Material Modeling

Steel frame members, comprising beams and columns, are built of A992 steel. The steel panels are made of ASTM A1008 steel, and the post-tensioned (PT) strands are made of ASTM A416. The materials specifications employed in the model are given in Table 1. Since only web plates will experience the plastic zone and frame members will remain elastic, the nonlinear behavior of materials is considered only for the web plate material.

[DOR: 20.1001.1.23454296.2022.6.4.8.5]
[DOI: 10.52547/nmce.6.4.67]

[DOR: 20.1001.1.23454296.2022.6.4.8.5]

[DOI: 10.52547/nmce.6.4.67]

3.2. Contact Surfaces

In order to model the interaction between the steel panel and the frame members, a tie constraint is employed. A tie constraint ties two separate surfaces together so that there is no relative motion between them. Considering that the welded components do not experience damage during the experiment, applying a tie constraint rather than modeling the welds does not affect the analysis response. A tie constraint is also exploited to simulate the connection of the strand end to the end edge of the column.

Because the beam-to-column connection is a simple web angle connection, and post-tensioned (PT) strands provide the fixed connection, the coupling constraint is used to simulate the beam-column connection. In this case, only the gravity loads are transmitted, and the connection is modeled as a simple connection.

Modeling the functioning of the rocking connection is carried out by creating a gap at the connection point. This spacing is put at points A, B, C, and D of Fig. 3 with a gap equal to 5 mm to model the rocking connection.

While lateral force is applied to the frame from right to left, the upper edge at the right side of the beam and the lower flange and left side of the beam (points A and B) are the ones that transmit the force, and a gap is created in the other two angles (points C and D), and the force is not transmitted. Hence, the modeling of the force transmission process should be such that force is transmitted in the pressure and operates in a neutral manner in tension. This means that the spacing placed at these points must be solely executed in the form of a pressurized spring, and the axial force transmission is carried out by these springs. The simulation of these springs is done by the create connector section, and only the axial force is introduced in the force transmission section. As these springs only operate under pressure, their properties are proposed so that their tensile strength against compressive strength is insignificant. Details of the beam-column connection are shown in Fig. 5. The axial springs are also shown with yellow triangles.

Table 1: Material properties

Element	Material	Young's modulus (MPa)	Poisson's ratio	Yield stress (MPa)	Ultimate stress (MPa)
Beam	ASTM A992	2×10^5	0.3	345	496
Column	ASTM A992	2×10^5	0.3	345	496
Cable	ASTM A416	1.96×10^5	0.3	1620	1900
Web panels	ASTM A1008	2×10^5	0.3	180	430

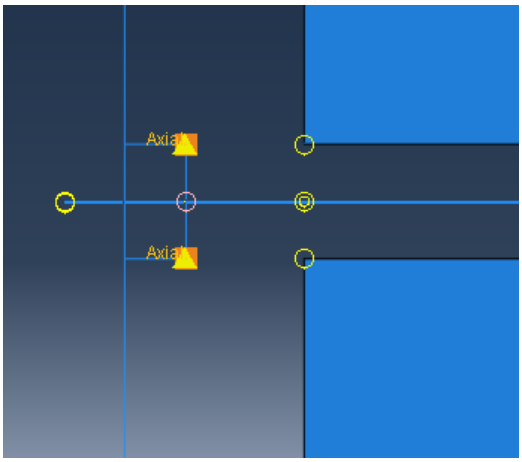

Fig. 5: Details of the beam-column connection in the finite element model

After introducing the specifications of the springs, they are deployed at gap spaces of 5 mm, already generated in the model. Indeed, these springs are placed at the connection point of the top and bottom edges of the beam to the column, and force is applied to one of these edges (compression edge) during the loading, and the other edge (tensile edge) does not transmit force.

3.3. Element Type and Mesh

As mentioned before, the self-centering steel plate shear wall is modeled using shell and wire elements rather than solid elements. Since shell and wire elements are used, the results are not much dependent on the mesh size, and according to the mesh size sensitivity analysis, by changing the mesh size, there was a minimal change in results. Therefore, the mesh dimension is selected as 50 mm in the model, which is an efficient value, considering the time of the analysis and accuracy of the results.

S4R, a linear 4-sided shell element, was used for meshing the web panels. S4R is a robust, general-purpose element suitable for a wide range of applications. In addition, B31 and T3D2 elements, which are 2-node linear elements, were used for meshing frame members and cables, respectively.

3.4. Boundary Conditions and Loading

Pinned boundary conditions are intended for the legs of both columns. In this case, the possibility of displacement in all directions is blocked, but free rotation is possible. For the assignment of the mentioned support conditions, the tie constraint of the rigid body was used. The pre-stressing force of cables was simulated in the model by a drop in temperature and thermal loading. The calculation procedure of the rate of temperature drop to generate the pre-stressing force is provided by the following equations:

$$\frac{PL}{AE} + \alpha L \Delta T = 0 \quad (3)$$

where P is the axial force, L is the length of the axial element, A is the area of the element, E is Young's modulus, and ΔT is temperature change. With respect to the information listed in the paper, the pre-stressing force is 334 kN, and the number of cables is 8. Considering α equal to 12×10^{-6} and the total area of the cables equal to 1061 square millimeters, the amount of temperature change to create the pre-stressing force is calculated to be 133 °C using Eq. (3).

Concerning the dissipation of pre-stressing force resulting from the shortening of the beam, the amount of these losses should be calculated, and the temperature should be dropped a little more such that the force losses are compensated. For pre-stressed elements:

$$T_s = T_0 + \Delta T \quad (4)$$

T_0 is the initial pre-stress force applied during the fabrication of the system, and ΔT represents the cable pre-stressing force losses.

The pre-stressing force losses caused by the shortening of HBE are due to the compressive axial force of the column; moreover, the compressive axial force results from the elongation of the pre-stressed elements during the opening of the connection [3]. The value of axial shortening of the beam is computed from the following equation:

$$\Delta_{loss} = \frac{P_{PT}}{k_{HBE}} + \frac{P_{HBE(VBE)}}{k_{HBE}} \quad (5)$$

In the above equation, P_{PT} is the compressive axial force applied to HBE from the pre-stressed elements, and $P_{HBE(VBE)}$ is the compressive axial force applied to HBE from the column. By solving the above equation, the following equation will be achieved:

$$P_{PT} = k_{HBE}\Delta_{loss} - P_{HBE(VBE)} \quad (6)$$

Accordingly, the net effective tensile force in a pre-stressed element is equal to:

$$T_{PT} = k_{PT}(\Delta_{drift} - \Delta_{loss}) \quad (7)$$

In the above equation, Δ_{drift}, which is associated with the elongation of the cables and the connection opening, equals to:

$$\Delta_{drift} = \emptyset_{drift} d \quad (8)$$

$\emptyset_{drift}$ is the relative angle between HBE and VBE, and d is equal to the beam depth. As $T_{PT} = P_{PT}$, the value of Δ_{loss} is equal to:

$$\Delta_{loss} = \frac{P_{HBE(VBE)}}{k_{HBE}+k_{PT}} + \left(\frac{k_{PT}}{k_{HBE}+k_{PT}}\right)\Delta_{drift} \quad (9)$$

Δ_{drift} is equal to the gap assumed in the finite element model, which is 5 mm, k_{PT} is the axial stiffness of cables and equal to 726 N/mm, k_{HBE} is the axial stiffness of the beam and equal to 1195 kN/mm. Therefore, Δ_{loss} is calculated as 0.6 mm.

Eventually, T_s that also includes losses caused by the beam shortening is equal to:

$$T_s = T_0 + \Delta T = T_0 + \frac{A_{PT}E_{PT}}{L_{PT}}\left(\Delta_{drift} - \Delta_{loss}\right) \quad (10)$$

Regarding the above equation, T_0 is the initial pre-stress force applied during the fabrication of the system, which is 334 kN, and ΔT represents the cable pre-stressing force loss, which is 35 kN, therefore T_s is 369 kN, and a drop in temperature at a rate of 147 degrees is desirable to create the 369 kN pre-stressing force.

In the experiment performed by Clayton et al. [17], the imposed loads are applied by a driving force to the top of the column. The loading protocol is according to ATC-24 [18]. The history of cyclic lateral displacement protocol per ATC-24 is demonstrated in Fig. 6. The finite element (FE) model is tested for up to 4% lateral displacement.

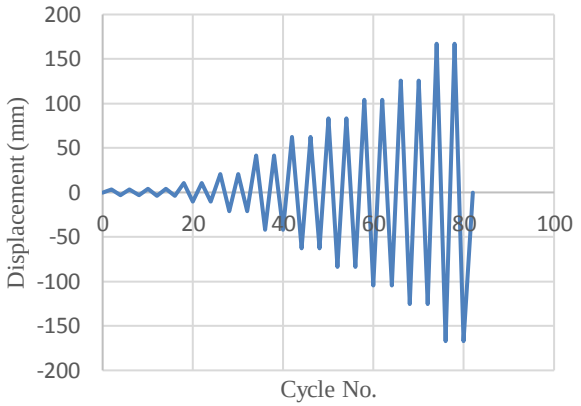

Fig. 6: The cyclic loading protocol for the SC-SPSW, based on ATC-24 [18]

The applied loadings comprise the initial defect load in the center of the panel as a concentrated load and the load under displacement control at the top of the column.

[DOR: 20.1001.1.23454296.2022.6.4.8.5]
[DOI: 10.52547/nmce.6.4.67]

The analysis is conducted in three time steps. The initial defect in the first step is generated by applying a concentrated load to the panel and buckling analysis. Next, the pre-stressing force is applied to the cables in the second step by applying the thermal load. Finally, a cyclic load is applied to the model in the form of displacement in the third step. Figure 7 represents the configuration of the FE modeling for analysis under cyclic loading.

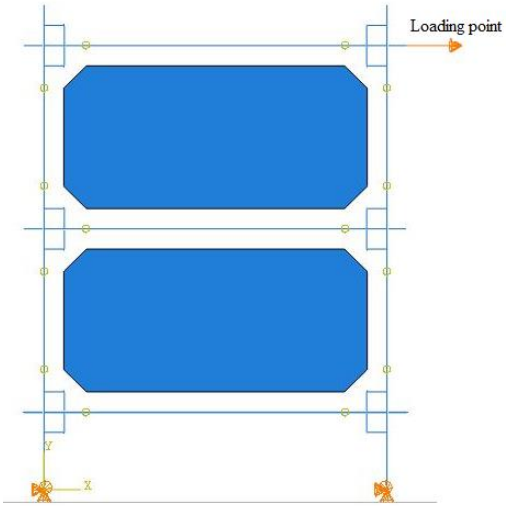

Fig. 7: SC-SPSW model configuration

3.5. Results and Verification

The results of the hysteresis analysis of the FE model are compared to those of the experimental model conducted by Clayton et al. [17] in Fig. 8. The lateral force and the drift ratios were measured at the top corner of the right column. It is clear that the finite element model is accurate and can verify the experimental model.

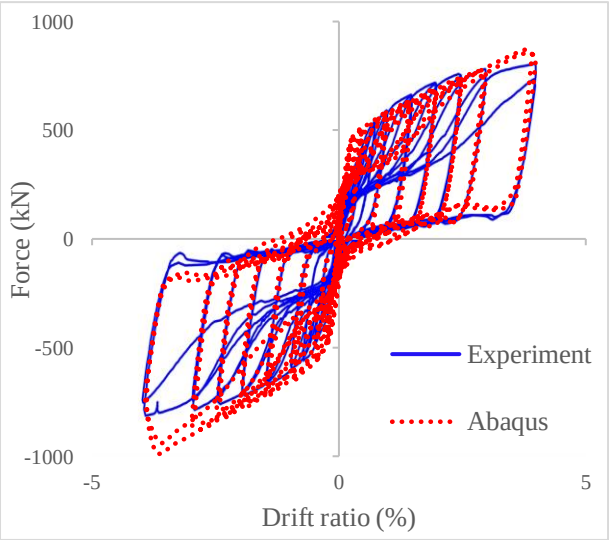

Fig. 8: Comparison of the hysteresis response of the experimental and numerical models

4. Fire loading

In this section, the behavior of the SC-SPSW under fire load is explored by using finite element analysis (FEA), and the results will be presented in the form of push-over curves.

For modeling the self-centering connection behavior under the effect of fire loading, its finite element method (FEM) should be varied. In order to simulate the behavior of materials at high temperatures, the Eurocode 3 reduction factor [19] was employed, and a fixed load was applied to the point specified in Fig. 7 rather than a cyclic load. Since fire generally happens after earthquake events and the structure will not experience fire and cyclic loading simultaneously, monotonic loading is performed to investigate the system's behavior under fire loading. Strength-reduction factors and modulus of elasticity are displayed in Table 2 according to Eurocode 3 and the fire diagram provided in Fig. 9.

As indicated in Table 2 and Fig. 9, the steel strength-reduction factors up to a temperature of 400 °C are equal to 1, and strength reduction is not expected until the temperature of 400 °C.

Table 2: Strength and Young's modulus reduction factors [19]

Steel temperature (C)	Reduction factor for yield stress	Reduction factor for Young's modulus
20	1	1
100	1	1
200	1	0.9
300	1	0.8
400	1	0.7
500	0.78	0.6
600	0.47	0.31
700	0.23	0.13
800	0.11	0.09
900	0.06	0.068
1000	0.04	0.045
1100	0.02	0.023
1200	0	0

[DOR: 20.1001.1.23454296.2022.6.4.8.5]
[DOI: 10.52547/nmce.6.4.67]

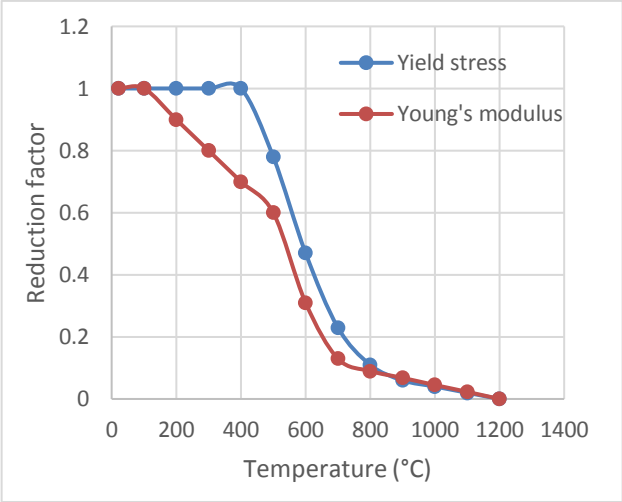

Fig. 9: Fire diagram in accordance with Eurocode 3 [19]

The analysis is carried out in three steps. In the first step, a concentrated load is applied to the panel for the buckling analysis. In the second step, the strands are post-tensioned by reducing temperature. Finally, in the third step, the temperature is increased up to a specified value, and the monotonic point load is inserted in the form of displacement.

The lateral strength of the system is approximately 400 kN at a temperature of 20 degrees. The strength does not exhibit much reduction by increasing the temperature up to 400 degrees, and it reaches nearly 100 kN at a temperature of 700 degrees. The push-over curve of the system under fire loading at different temperatures is illustrated in Fig. 10.

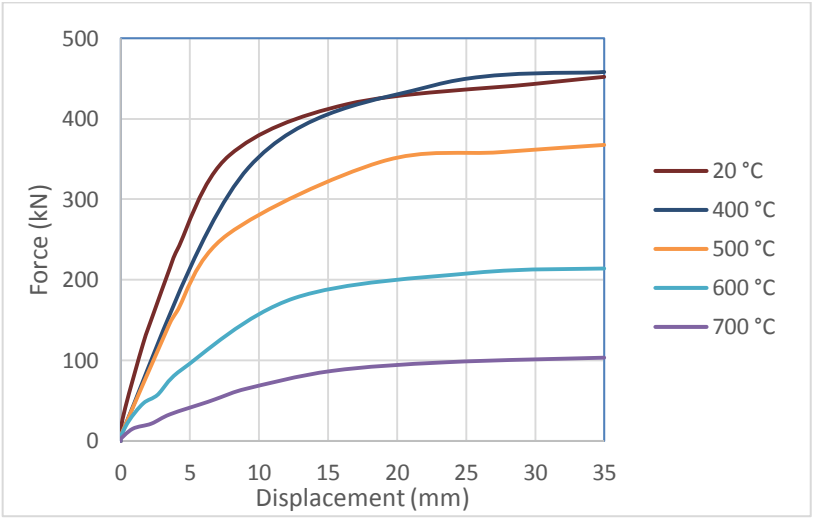

Fig. 10: Force-displacement curve of the SC-SPSW model at different temperatures

In the next scenario, the protection coating against fire is employed in three steps, once for steel panels, once for post-tensioned (PT) strands, and once for both panels and strands simultaneously. The coating used for fire protection is a cement-based material with a thickness of 3-5 mm. The fire-resistant cement could be utilized as a fire protection coating, which can insulate a steel member against fire for up to 4 hours, depending on its thickness. It should be mentioned that the coating is not modeled in Abaqus, but its protecting effects are considered in the material properties of other elements. The analysis of all three scenarios was carried out at temperatures of 20, 400, 500, 600, and 700 degrees Celsius. The push-over curves of the system at various temperatures for all three scenarios are demonstrated in Fig. 11

[DOR: 20.1001.1.23454296.2022.6.4.8.5]
[DOI: 10.52547/nmce.6.4.67]

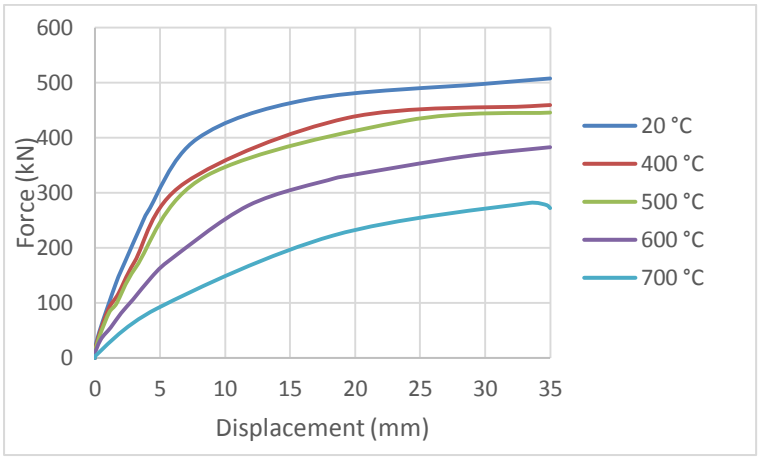

(a)

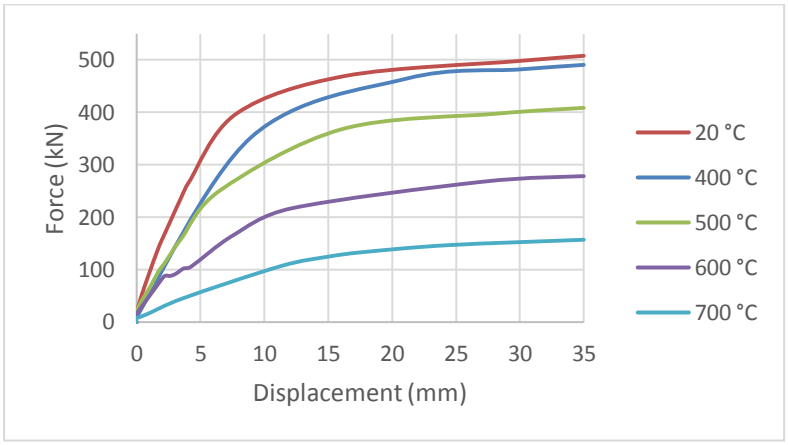

(b)

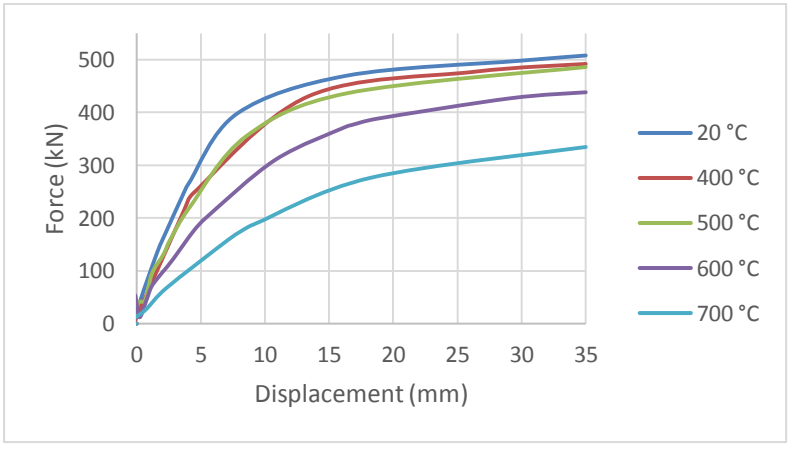

(c)

Fig. 11: Force-displacement curves under different temperatures for (a) SC-SPSW model with coating on steel panels, (b) SC-SPSW model with coating on PT cables, (c) SC-SPSW model with coating on both steel panels and PT cables

The curves of both models have a slight difference from each other at the temperatures of 20 °C and 400 °C. This indicates that the protected models exhibit more lateral strength by an enhancement in temperature as long as there is no significant drop in the properties of steel materials. The variations of the maximum lateral strength at temperatures of 500, 600, and 700 °C are shown in Fig. 12. It can be deducted that the existence of a protector for the

[DOR: 20.1001.1.23454296.2022.6.4.8.5]
[DOI: 10.52547/nmce.6.4.67]

panels provides a more significant impression on enhancing the model strength compared to the scenario in which cables are equipped with a protective coating.

As demonstrated in Fig. 12, the protected models reveal much better behavior relative to unprotected models by an increase in temperature and a drop in properties of steel materials such that the maximum lateral strength of the model with shielded steel panels, the model with shielded strands, and the model with simultaneously shielded strands and steel panels are respectively 56%, 21%, and 61% greater than the model without shields at a temperature of 700 °C. Force-displacement curves at 700 °C for models with coating on cables and panels and the model without any coating are shown in Fig. 13

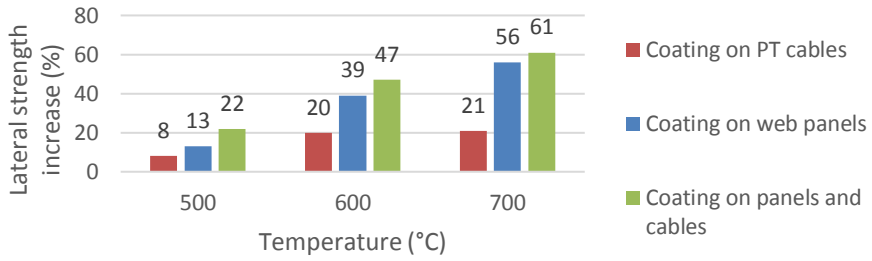

Fig. 12: Increased lateral resistance of shielded models at different temperatures

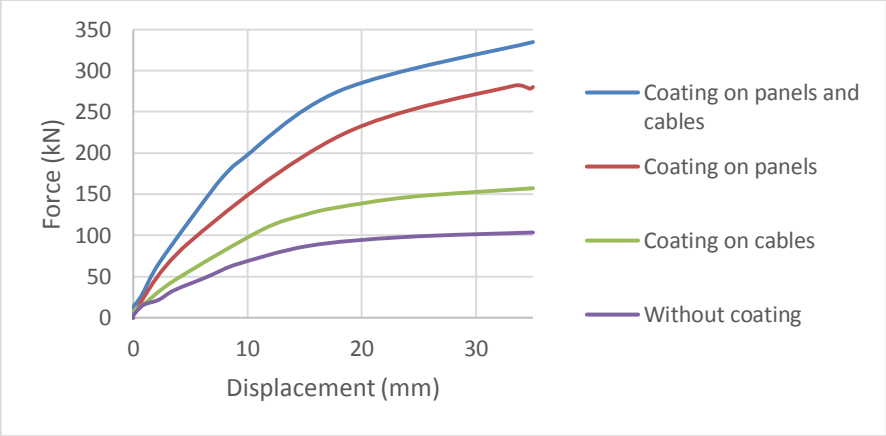

Fig. 13: Force-displacement curves at 700 °C for models with coating on cables and panels and the model without any coating

It can be inferred from the investigation of the force-displacement responses at various states and temperatures that applying the protective coating for panels and strands substantially influences the performance of the self-centering shear wall and upgrades its performance under fire loads.

4.1. Discussion

Based on Eurocode reduction factors, as the temperature increases, the yield stress and Young's modulus of the material decrease. The yield strain can be computed through Eq. (11).

$$\varepsilon_y = \frac{\sigma_y}{E} \tag{11}$$

where σ_y is the yield stress, and E is Young's modulus. By applying the reduction factors on σ_y and E, the yield strain-temperature curve can be obtained, as shown in Fig. 14. It is evident that by increasing the temperature from 20 °C to 700 °C, the yield strain will increase; thus, the model will enter the nonlinear zone at higher displacements.

The force-displacement curves of the unprotected model at 400 °C and 700 °C are shown in Fig. 15. At 400 °C, the model enters the nonlinear zone with a displacement of 5 mm. However, at 700 °C, this value increases to 10 mm.

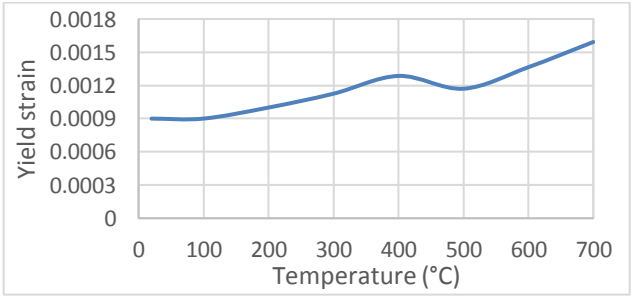

Fig. 14: Yield strain-temperature curve based on Eurocode 3 reduction factors

[DOR: 20.1001.1.23454296.2022.6.4.8.5]
[DOI: 10.52547/nmce.6.4.67]

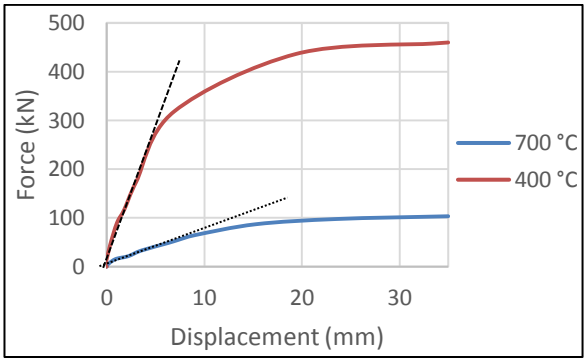

Fig. 15: Force-displacement curve of the unprotected model at 700 °C and 400 °C

5. Conclusion

This research presents a novel steel plate shear wall system called self-centering steel plate shear wall (SC-SPSW). First, the mechanics of the proposed system were presented. Then, the hysteretic response of the SC-SPSW was examined under the cyclic loading protocol developed by ATC-24. The results were verified using the two-story experimental model presented by Clayton et al. Moreover, a numerical study was performed to investigate the performance of SC-SPSW under fire loading. Force-displacement curves in 20, 400, 500, and 700 °C showed that in temperatures above 400 °C, the lateral strength of the system dropped significantly. Results showed that by using fire-resistant coating on web panels, cables, and both panels and cables, the lateral strength of the SC-SPSW system becomes respectively 56%, 21%, and 61% greater than that of the model without fire-resistant coating at 700 °C.

As for future work, any experimental investigation on the performance of the mentioned system to compare numerical and experimental results is highly recommended for further studies on the self-centering steel plate shear wall.

References

[1] D. K. Miller, "Lessons learned from the Northridge earthquake," *Eng. Struct.*, vol. 20, no. 4–6, pp. 249–260, 1998, doi: 10.1016/S0141-0296(97)00031-X.

[2] M. D. Engelhardt and T. A. Sabol, "Reinforcing of steel moment connections with cover plates: Benefits and limitations," *Eng. Struct.*, vol. 20, no. 4–6, pp. 510–520, 1998, doi: 10.1016/S0141-0296(97)00038-2.

[3] D. M. Dowden, R. Purba, and M. Bruneau, "Behavior of Self-Centering Steel Plate Shear Walls and Design Considerations," *J. Struct. Eng.*, vol. 138, no. 1, pp. 11–21, 2012, doi: 10.1061/(ASCE)st.1943-541x.0000424.

[4] F. J. Perez, R. Sause, S. Pessiki, and L.-W. Lu, "Lateral load behavior of unbonded post-tensioned precast concrete walls," *Adv. Build. Technol.*, pp. 423–430, 2002, doi: 10.1016/b978-008044100-9/50055-3.

[5] J. I. Restrepo, J. Mander, and T. J. Holden, "New Generation of Structural Systems for Earthquake Resistance," *New Zeal. Soc. Earthq. Eng. 2001 Conf.*, pp. 1–9, 2001.

[6] J. I. Restrepo and A. Rahman, "Seismic Performance of Self-Centering Structural Walls Incorporating Energy Dissipators," *J. Struct. Eng.*, vol. 133, no. 11, pp. 1560–1570, 2007, doi: 10.1061/(ASCE)0733-9445(2007)133:11(1560).

[7] N. H. Hamid and J. B. Mander, "Lateral Seismic Performance of Multipanel Precast Hollowcore Walls," *J. Struct. Eng.*, vol. 136, no. 7, pp. 795–804, 2010, doi: 10.1061/(ASCE)st.1943-541x.0000183.

[8] P. M. Clayton, D. M. Dowden, T. Winkley, J. W. Berman, M. Bruneau, and L. N. Lowes, "Experimental investigation of self-centering steel plate shear walls," *Struct. Congr. 2012 - Proc. 2012 Struct. Congr.*, pp. 1586–1597, 2012, doi: 10.1061/9780784412367.141.

[9] E. Nobahar, B. Asgarian, A. Torabi Goodarzi, and O. Mercan, "Optimal placement of post-tensioned self-centering yielding braced systems for braced frame structures," *Numer. Methods Civ. Eng.*, vol. 4, no. 2, pp. 17–35, 2019, doi: 10.52547/nmce.4.2.17.

[10] J. Liu, L. Xu, and Z. Li, "Development and experimental validation of a steel plate shear wall with self-centering energy dissipation braces," *Thin-Walled Struct.*, vol. 148, 2020, doi: 10.1016/j.tws.2019.106598.

[11] T. Hitaka and C. Matsui, "Experimental Study on Steel Shear Wall with Slits," *J. Struct. Eng.*, vol. 129, no. 5, pp. 586–595, 2003, doi: 10.1061/(ASCE)0733-9445(2003)129:5(586).

[12] W. Wang, J. Kong, Y. Zhang, G. Chu, and Y. Chen, "Seismic Behavior of Self-Centering Modular Panel with Slit Steel Plate Shear Walls: Experimental Testing," *J. Struct. Eng.*, vol. 144, no. 1, p. 04017179, 2018, doi: 10.1061/(ASCE)st.1943-541x.0001932.

[13] A. A. Kajbaf. N Fanaie, "Investigation on the Influence of Posttensioned Strands on the behavior of SelfCentering Connection under Fire Loading," 2018.

[14] S. Ni and A. C. Birely, "Post-fire seismic behavior of reinforced concrete structural walls," *Eng. Struct.*, vol. 168, pp. 163–178, 2018, doi: 10.1016/j.engstruct.2018.04.018.

[15] F. Mazza, "Behaviour during seismic aftershocks of r.c. base-isolated framed structure with fire-induced damage," *Eng. Struct.*, vol. 140, pp. 458–472, 2017, doi: 10.1016/j.engstruct.2017.03.008.

[16] L. Jin, X. Li, R. Zhang, and X. Du, "Meso-scale modelling the post-fire seismic behavior of RC short columns," *Eng. Fail. Anal.*, vol. 120, 2021, doi: 10.1016/j.engfailanal.2020.105117.

[17] P. M. Clayton, J. W. Berman, and L. N. Lowes, "Subassembly testing and modeling of self-centering steel plate shear walls," *Eng. Struct.*, vol. 56, pp. 1848–1857, 2013, doi: 10.1016/j.engstruct.2013.06.030.

[18] "ATC. Guidelines for seismic testing of components of steel structures. Tech. Rep. 24. Applied Technology," 1992.

[19] "Brussels: European Committee for Standardization DD ENV; 3: Design of steel structures–Part 1.2: General rules–Structural fire design, E. Eurocode," 1993.